JACS Au
AN OPEN ACCESS JOURNAL OF THE AMERICAN CHEMICAL SOCIETY

pubs.acs.org/jacsau

Article

Periodic Arrays of Metal Nanoclusters on Ultrathin Fe-Oxide Films Modulated by Metal-Oxide Interactions

Xuda Luo, Xiaoyuan Sun, Zhiyu Yi, Le Lin, Yanxiao Ning,* Qiang Fu,* and Xinhe Bao

Cite This: *JACS Au* 2023, 3, 176−184

Read Online

ACCESS | Metrics & More | Article Recommendations | Supporting Information

ABSTRACT: Rational design of highly stable and active metal catalysts requires a deep understanding of metal−support interactions at the atomic scale. Here, ultrathin films of FeO and FeO_{2-x} grown on Pt(111) are used as templates for the construction of well-defined metal nanoclusters. Periodic arrays of Cu clusters in the form of monomers and trimers are preferentially located at FCC domains of FeO/Pt(111) surface, while the selective location of Cu clusters at FeO_2 domains is observed on FeO_{2-x}/Pt(111) surface. The preferential nucleation and formation of well-ordered Cu clusters are driven by different interactions of Cu with the Fe oxide domains in the sequence of FeO_2-FCC > FeO-FCC > FeO-HCP > FeO-TOP, which is further validated by density functional theory calculations. It has been revealed that the *p*-band center as a reactivity descriptor of surface O atoms determines the interaction between metal adatoms and Fe oxides. The modulated metal-oxide interaction provides guidance for the rational design of supported single-atom and nanocluster catalysts.

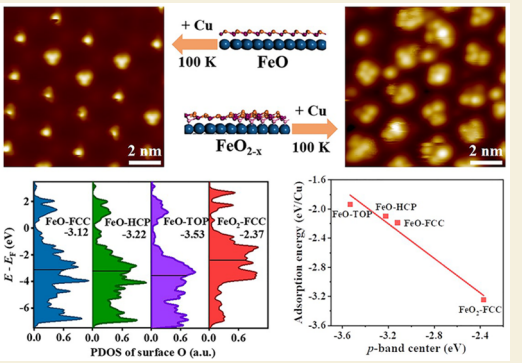

KEYWORDS: *metal-oxide interaction, p-band center, Cu nanoclusters, Fe oxide films, scanning tunneling microscopy*

INTRODUCTION

Single-atom and nanocluster catalysts have attracted great attention due to their high catalytic performance and atom utilization efficiency.[1−3] The precise size control of single-atom and nanocluster catalysts and their stability during reactions remain a great challenge due to their high surface energy and strong tendency toward aggregation. Oxides are widely used as supports for metal atoms and nanoclusters in industrial catalysis and play a critical role to anchor these active nanostructures. Further, metal-oxide interactions can modulate the electronic structures and catalytic performance of supported metal catalysts,[4−6] and the formed metal-oxide interfaces show a catalytic synergistic effect to present high catalytic activity and selectivity.[7−9] Consequently, the interaction between metal atoms/nanoclusters and oxide supports has been extensively investigated in heterogeneous catalysis. It has been well recognized that the metal-oxide interaction can be effectively tailored by surface structures of oxide supports such as crystal face,[10,11] surface defects,[12,13] and surface functional groups.[14] Nevertheless, the fundamental understanding of the metal-oxide interaction and interfacial bonding still deserves further exploration.

In real heterogeneous catalytic systems, the structures of metal on oxide supports are very complex. It is difficult to obtain a deeper understanding of the metal-oxide interaction at the atomic scale, which can be explored by model catalyst systems with fewer variables and controllable structures. Oxide single crystals such as TiO_2(110)[15,16] and Fe_3O_4(001)[17,18] have been used as supports for metal nanostructures to explore metal-oxide interactions. However, the poor conductivity of most oxide bulks limits their application for surface science characterizations. Ultrathin oxide films supported on metal single crystals are also applied to support single atoms or nanoclusters,[19−21] allowing atomic resolution of surface structures by surface analytic techniques. In addition, two-dimensional oxide films grown on metal surfaces often show moiré superstructures due to the lattice mismatch between oxide overlayers and metal surfaces, which can be used as templates for the construction of ordered metal atoms and nanoclusters,[22,23] similar to previous findings of well-ordered metal nanoclusters supported on graphene[24,25] and hexagonal boron nitride.[26,27] On the basis of well-defined metal atoms and nanoclusters supported on ultrathin oxide films, the coordination environment and electronic structures of metal nanostructures can be definitely characterized, allowing us to understand the metal-oxide interaction at the atomic scale.

Ultrathin FeO film grown on Pt(111) has a moiré structure with different stacking configurations, including face-centered cubic (FCC), hexagonal close-packed (HCP), and TOP

Received: October 22, 2022
Revised: November 30, 2022
Accepted: December 7, 2022
Published: December 21, 2022

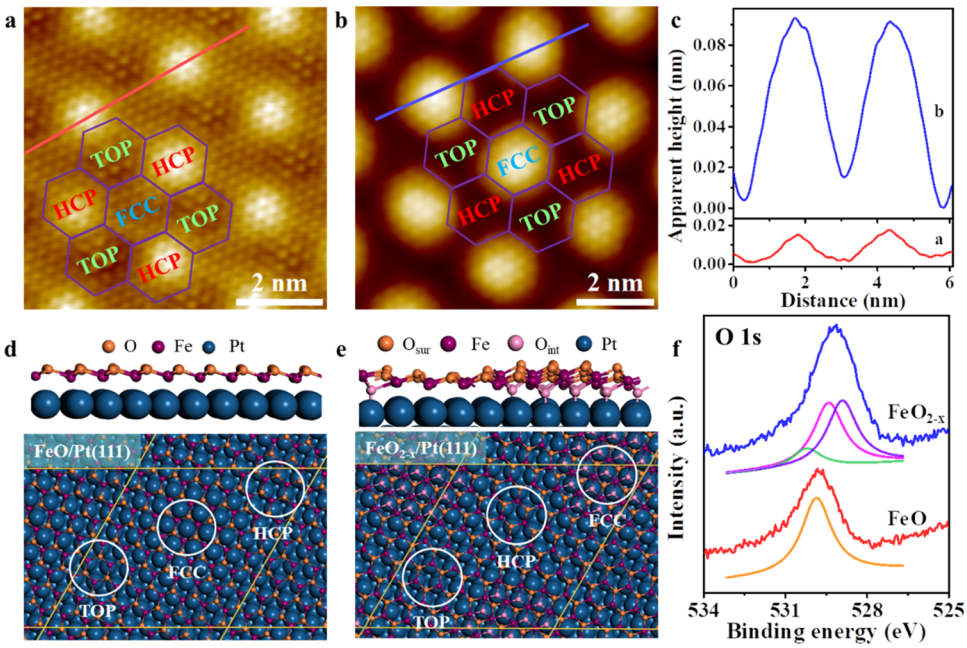

Figure 1. Atomically resolved STM images of FeO/Pt(111) (a) (7 × 7 nm^2; I = 0.5 nA, V = 0.1 V) and FeO$_{2-x}$/Pt(111) (b) (7.8 × 7.8 nm^2; I = 0.1 nA, V = 0.1 V); FCC, HCP and TOP domains are labeled in the images. (c) Line profiles of FeO (lower) and FeO$_{2-x}$ (upper) surfaces, corresponding to the red and blue lines in panels (a, b), respectively. Top and side views of the optimized structures of FeO/Pt(111) (d) and FeO$_{2-x}$/Pt(111) (e) superstructures of ($\sqrt{84}$ × $\sqrt{84}$)R10.9° indicated by a yellow parallelogram. The white circles mark the three different domains. Pt: dark blue; Fe: purple; surface O: orange; and interface O: pink. Notably, the HCP and TOP domains of the FeO$_{2-x}$/Pt(111) surface have the same O−Fe bilayer structures as those of the FeO/Pt(111) surface. (f) XPS O 1s spectra of the FeO/Pt(111) (red) and FeO$_{2-x}$/Pt(111) (blue) surfaces; fitting peaks of FeO$_{2-x}$ in purple, pink, and green represent surface lattice oxygen, interface lattice oxygen, and surface hydroxyl, respectively.

domains, where different Fe−O layer distances and surface dipoles have been reported.[28−32] An FeO/Pt(111) surface has been used as a template for the construction of well-ordered Au atom arrays and most Au atoms are located at FCC domains.[33,34] FeO/Pt(111) can be oxidized into FeO$_{2-x}$/Pt(111),[35−38] which also has a superstructure similar to FeO/Pt(111)[36] and is another potential template for the growth of metal cluster arrays. Surface O atoms in FeO and FeO$_{2-x}$ films have nearly identical coordination structures and lattice parameters but present different activity for CO oxidation,[36,38] which may show different interactions with metals. The well-defined FeO and FeO$_{2-x}$ films with similar O-terminated surfaces offer ideal models to understand how the surface O property influences metal-oxide interactions.

In the present work, atomically flat FeO and FeO$_{2-x}$ films on Pt(111) were used as templates for the growth of Cu atoms and clusters. Scanning tunneling microscopy (STM) investigations indicate that Cu atoms prefer to locate at FCC domains of the FeO film and FeO$_2$ domains of the FeO$_{2-x}$ film, forming well-ordered Cu nanocluster arrays. Density functional theory (DFT) calculations show the adsorption strengths of Cu atoms on different domains of FeO$_x$ following the sequence of FeO$_2$-FCC > FeO-FCC > FeO-HCP > FeO-TOP. The interaction is determined by the reactivity of surface O atoms in the Fe oxide films, which can be described by the p-band center.

METHODS

Experimental Details

All experiments were performed in a two-chamber ultrahigh vacuum (UHV) system. The preparation chamber comprises X-ray photoelectron spectroscopy (XPS), evaporators, and cleaning facilities. XPS spectra were acquired using a dual-anode X-ray source (SPECS) with Mg Kα (1253.6 eV) and Al Kα (1486.6 eV) radiation. A CreaTec low-temperature STM (LT-STM) is equipped in the STM chamber. The temperature of STM measurement is held at 78 K. The base pressures of the STM and preparation chambers are 5 × 10^{-11} and 1 × 10^{-10} mbar, respectively.

A Pt(111) single crystal (MaTeck) was cleaned by cycles of Ar$^+$ sputtering (1 keV, 10 μA) and annealing at 1050 K in UHV. When needed, the sample was annealed in 1 × 10^{-7} mbar O_2 at 700 K to remove carbon species on the Pt(111) surface. The clean Pt(111) surface was checked by STM. The FeO film was grown on Pt(111) by deposition of Fe atoms from a Knudsen cell (CreaTec) in an O_2 atmosphere with Pt(111) held at room temperature (RT) and annealing in an O_2 atmosphere afterward. To get the FeO$_{2-x}$/Pt(111) film, the FeO/Pt(111) surface was exposed to O_3 at RT and then annealed in UHV. O_3 dosing composed of 10% O_3 and 90% O_2 was generated by a high-purity ozone generator system.[39,40] Cu was evaporated from another Knudsen cell (CreaTec), and Ce was evaporated from an e-beam evaporator (SPECS) with controllable evaporation flux onto FeO or FeO$_{2-x}$ surfaces, which were held at 100 K or RT. STM images were processed with SPIP software.

Computational Details

Spin-polarized DFT calculations were implemented using a plane-wave basis set in the Vienna Ab initio Simulation Package (VASP 5.4).[41] The exchange−correlation energy was treated using the Perdew−Burke−Ernzerhof (PBE) functional within the generalized gradient approximation (GGA).[42] The projected-augmented wave (PAW) pseudopotentials were utilized to describe the core electrons, and a cutoff energy of 400 eV was used for the plane-wave expansion.[43] The following valence electron configurations were included in the self-consistent field calculations: Pt (5d^9 and 6s^1), Cu (3d^{10} and 4s^1), Fe (3d^6 and 4s^2), and O (2s^2 and 2p^4). In addition, the van der Waals (vdW) dispersion forces were corrected by the vdW−DF (optPBE) functionals, which showed a highly accurate description of oxides.[44,45] An on-site Hubbard term U_{eff} = U − J was added to

https://doi.org/10.1021/jacsau.2c00580
JACS Au 2023, 3, 176−184

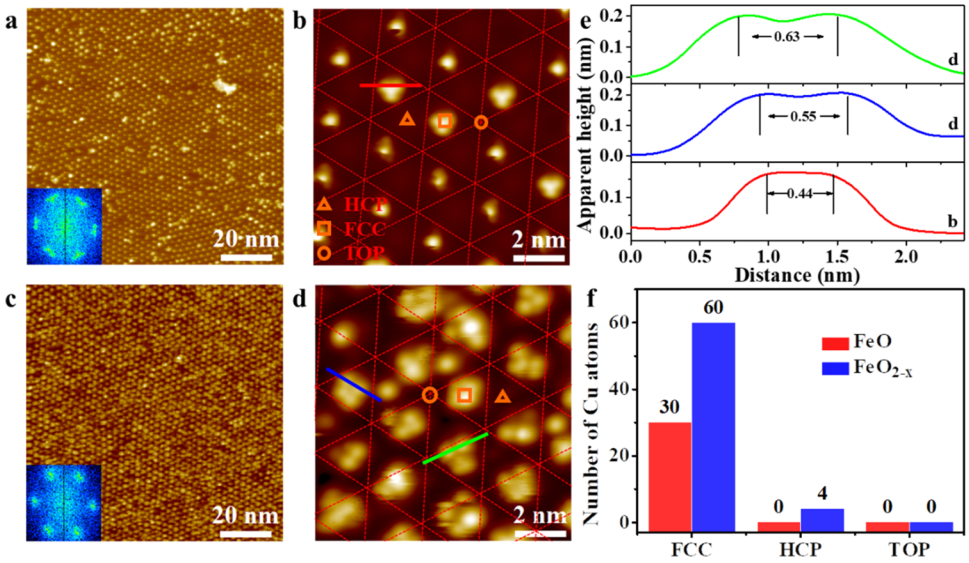

Figure 2. STM images of 0.05 ML Cu deposited at 100 K on FeO/Pt(111) (a) (100 × 100 nm^2; I = 0.01 nA, V = 1 V) and (b) (10 × 10 nm^2; I = 0.1 nA, V = 0.3 V), and FeO_{2-x}/Pt(111) (c) (100 × 100 nm^2; I = 0.01 nA, V = 1 V) and (d) (10 × 10 nm^2; I = 0.1 nA, V = 0.5 V). The insets in panels (a, c) are their corresponding FFT images. FCC, HCP, and TOP domains are marked by squares, triangles, and circles, respectively. (e) Line profiles of Cu atoms and distances between Cu atoms correspond to the red line in panel (b) and blue and green lines in panel (d), respectively. (f) Statistical histograms of the number of Cu atoms in different domains in (b, d).

address the open-shell d-electrons with 2.71 eV for Fe in FeO/Pt(111) and with 2.97 eV for Fe in FeO_{2-x}/Pt(111).[46] The water-based reference state for the calculations has been adopted to avoid an incorrect description of the gas phase O_2 reference with standard DFT methods.[44] The energies and residual forces were converged to 10^{-5} eV and 0.02 eV Å^{-1}, respectively.

The adsorption energy of Cu on FeO_x/Pt(111) is

$$E_{ads} = E_{FeO_x/Pt(111)+Cu} - E_{Cu} - E_{FeO_x/Pt(111)} \quad (1)$$

where E_{Cu}, $E_{FeO_x/Pt(111)}$, and $E_{FeO_x/Pt(111)+Cu}$ are the energies of Cu atoms in the gas phase, bare FeO_x/Pt(111), and the structures after Cu atom adsorption on FeO_x/Pt(111) surfaces, respectively.

The p-band center (ε_p) of surface O is defined as

$$\varepsilon_p = \frac{\int_{-\infty}^{\infty} n_p(\varepsilon)\varepsilon d\varepsilon}{\int_{-\infty}^{\infty} n_p(\varepsilon) d\varepsilon} \quad (2)$$

Model Constructions

We built up two basic models to corroborate the geometric structures of single-atom Cu located on FeO_x/Pt(111). The FeO/Pt(111) interface was modeled using a moiré superstructure ($\sqrt{84} \times \sqrt{84}$)R10.9°-FeO/Pt(111) with a period of 2.5 nm, which amounts to placing an FeO-($\sqrt{67} \times \sqrt{67}$) monolayer on a Pt(111)-($\sqrt{84} \times \sqrt{84}$) substrate with a three-layer thickness.[7,29,47,48] The FeO_{2-x}/Pt(111) interface was constructed by shifting the O sublattice of FeO/Pt(111) from one Fe hollow site to another and adding extra 19 O atoms into the Fe−Pt interlayer in FCC domains of the new FeO/Pt(111) surface, and the intercalated O atoms are located at Pt-top sites. During the structure relaxation, the FeO_x overlayer and the top two Pt layers were fully relaxed and the bottom Pt layer was constrained. The (1 × 1 × 1) k-point grids were exploited for all FeO_x/Pt(111) structures.

RESULTS AND DISCUSSION

Atomic Structures of FeO/Pt(111) and FeO_{2-x}/Pt(111) Surfaces

The full monolayer (ML) FeO film on Pt(111) was prepared by depositing Fe atoms in an O_2 atmosphere (1 × 10^{-7} mbar) onto the Pt(111) surface held at RT and then annealing in the O_2 atmosphere (5 × 10^{-8} mbar) at 730 K (Figure S1a). The atomically resolved STM image of the ML FeO film shows that a hexagonal moiré pattern (Figure 1a) with a periodicity of 2.5 nm (lower panel in Figure 1c) is formed due to the lattice mismatch between Pt(111) ($d_{Pt\text{-}Pt}$ = 0.27 nm) and FeO (d_{Fe-Fe} = 0.31 nm). According to the literature,[49−51] the FeO/Pt(111) surface features an O−Fe−Pt (from top to bottom) layered structure, as shown in Figure 1d. From the top view, the moiré patterns can be divided into three regions including FCC domains (both Fe and O on Pt-hollow sites), HCP domains (Fe on Pt-hollow site and O on Pt-top site), and TOP domains (Fe on Pt-top site and O on Pt-hollow site).[31] The attribution of different regions in STM images has been well established.[29,31,47,48]

The transformation of the FeO film into the FeO_{2-x} film has been achieved by atomic oxygen exposure at RT.[37] Here, we find that the FeO/Pt(111) surface can be oxidized into FeO_{2-x}/Pt(111) through the exposure of 30 L (Langmuir, 1 L = 1 × 10^{-6} Torr·s) O_3 at RT and subsequent annealing in UHV at 500 K to desorb weakly bound oxygen species (Figure S1b). Figure 1b displays an atomically resolved STM image of the FeO_{2-x} surface, which exhibits closely packed patterns with the same lattice spacing and moiré periodicity of the FeO/Pt(111) surface, but presents a larger surface corrugation (0.09 nm, upper panel in Figure 1c). According to the domain assignment in the STM image of a surface containing both unoxidized and oxidized regions (Figure S2), the brighter domains in the FeO_{2-x} film are identified to be located at FCC domains of the FeO film, which originates from intercalated oxygen at the Fe−Pt interface and formation of O−Fe−O trilayer structures, while HCP and TOP domains of the the FeO_{2-x}/Pt(111) surface remain as the O−Fe bilayer structures.[37,38,48] According to STM results, the atomic model of the FeO_{2-x}/Pt(111) surface was constructed and optimized (Figure 1e).[37] Notably, each Fe atom in FeO_2-FCC is sixfold-coordinated, which is higher than threefold-

https://doi.org/10.1021/jacsau.2c00580
JACS Au 2023, 3, 176−184

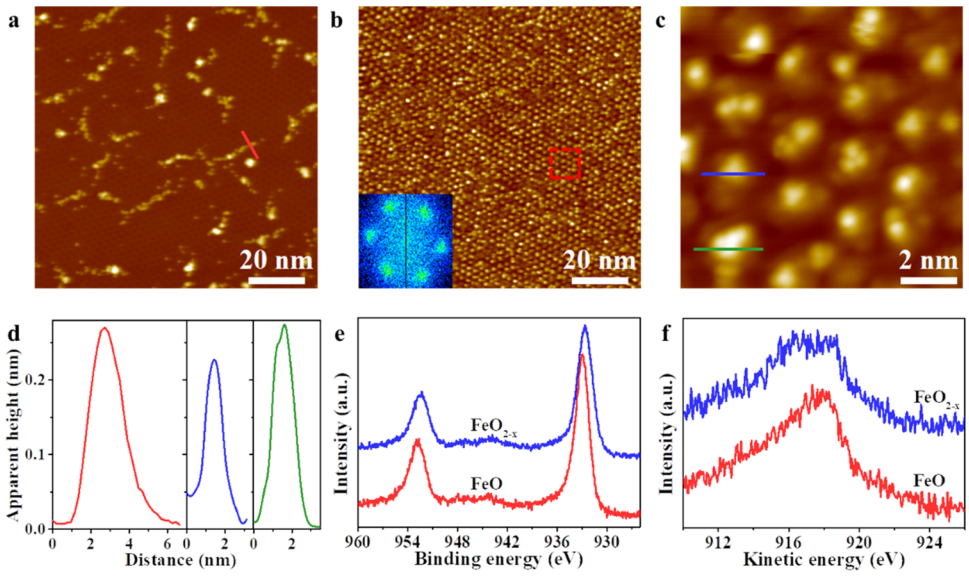

Figure 3. STM images of (a) 0.05 ML Cu deposited at RT on FeO/Pt(111) (100 × 100 nm^2; I = 0.01 nA, V = 1 V), (b) 0.05 ML Cu deposited at RT on FeO_{2-x}/Pt(111) (100 × 100 nm^2; I = 0.01 nA, V = 1 V), and (c) red square in panel (b) (10 × 10 nm^2; I = 0.1 nA, V = 0.3 V). The inset in panel (b) is its corresponding FFT image. (d) Line profiles of Cu nanostructures correspond to the red line in panel (a) and blue and green lines in panel (c), respectively. XPS Cu 2p spectra (e) and Cu LVV Auger spectra (f) of 0.5 ML Cu deposited on FeO/Pt(111) at 100 K and on FeO_{2-x}/Pt(111) at RT.

coordinated Fe in FeO-FCC, while the surface O atoms in both systems are all threefold-coordinated.

Following the oxidation of FeO into FeO_{2-x}, the XPS O 1s peak shifts to a lower binding energy (BE) position (Figure 1f).[35,52] Meanwhile, a larger full width at half-maximum can be seen in the spectrum, which means multiple components are present in it. It has been figured out that the surface oxygen has a lower BE compared with the interface oxygen in the O−Fe−O trilayer structures.[35] The deconvoluted components (blue spectrum in Figure 1f) show that the BEs of the surface oxygen and interface oxygen are 528.8 and 529.4 eV, respectively, and the small peak at 530.2 eV is attributed to hydroxylation of surface oxygen.[35]

Deposition of Cu on FeO/Pt(111) and FeO_{2-x}/Pt(111) at 100 K

After depositing 0.05 ML Cu on the FeO/Pt(111) surface at 100 K, highly ordered and dispersed clusters (0.16 count/nm^2) are formed on the surface (Figure 2a), while a few aggregated nanostructures also exist. Fast Fourier transformation (FFT) analysis of the STM image shows a nearly sixfold symmetric diffraction pattern with a periodicity of 2.6 nm, close to that of the moiré pattern of the FeO film. Stripes rather than dots in the FFT pattern indicate that the FeO film consists of domains with different rotation angles with respect to the Pt(111) surface, the same as that in Figure S1a. Cu nanostructures are in the form of either monomers with a height of 0.19 nm or trimers with a height of 0.17 nm (Figure 2b). The spacing between neighboring atoms of the trimer clusters is around 0.44 nm (Figure 2e). The spatial distribution of the monomers and trimers in the three domains has been statistically analyzed, and the data are shown in Figure 2f, which suggest that Cu atoms or clusters mainly anchor at FCC domains but scarcely at HCP and TOP domains. Thus, the FCC domains have the strongest interaction with Cu atoms, in line with Au atoms on FeO.[33,34]

Depositing 0.05 ML Cu on FeO_{2-x} at 100 K produces a higher density (0.38 count/nm^2) of Cu atoms and clusters and almost no aggregated islands on the FeO_{2-x} film (Figure 2c) in contrast with Cu deposition on the FeO film. The FFT image shows a sixfold symmetric diffraction pattern, which stems from the well-ordered Cu cluster arrays with a periodicity of 2.6 nm, close to that of the clean FeO_{2-x} surface (Figure S1b). The high-resolution STM image indicates that most of the clusters sit on FeO_2-FCC domains (Figure 2d) with a height of around 0.15 nm (Figure 2e). Only a few isolated Cu atoms are located on HCP domains but none of the Cu atoms are on TOP domains (Figure 2f). Each cluster sitting in the FeO_2-FCC domain consists of one or a few atoms, which are distributed randomly within the domain. The distances between neighboring Cu atoms are 0.55 and 0.63 nm, respectively (Figure 2e), which are larger than those of the Cu clusters on FeO. The thermal stability of the Cu nanostructures on FeO and FeO_{2-x} films has been investigated by annealing the as-prepared samples to RT. As shown in Figure S3, Cu atoms and clusters on FeO aggregate to form large clusters and nanoparticles with an irregular distribution, while the well-ordered Cu cluster arrays are still observed on the FeO_{2-x} surface, indicating higher thermal stability of Cu clusters on the FeO_{2-x} film.

Deposition of Cu on FeO/Pt(111) and FeO_{2-x}/Pt(111) at RT

Deposition of 0.05 ML Cu on the FeO/Pt(111) surface at RT induces a much less density of Cu clusters (0.02 count/nm^2) and aggregation of Cu atoms in the form of linear nanostructures (Figure 3a), which are selectively grown at the domain boundaries (Figure S4) and composed of nanoparticles with a length of several nanometers and a height of around 0.26 nm (Figure 3d). It is inferred that the interaction between the Cu and FeO film is so weak that the deposited Cu atoms can easily diffuse and aggregate on the FeO surface at RT. The XPS Fe 2p signal has almost no change after deposition of 0.7 ML Cu at RT (Figure S5a). The X-ray-induced Cu LVV Auger peak indicates that the deposited Cu atoms on FeO at RT are still metallic (Figure S5b). Therefore, the linear nanostructures observed in Figure 3a

https://doi.org/10.1021/jacsau.2c00580
JACS Au 2023, 3, 176−184

Table 1. Calculated Cu Adatom Adsorption Sites and Adsorption Energies (E_{ads}, eV)

domain	FeO-FCC			FeO-HCP			FeO-TOP			FeO_2-FCC		
initial configuration	O-fcc	O-hcp	O-top	O-fcc	O-hcp	O-top	O-fcc	O-hcp	O-top	O-fcc	O-hcp	O-top
optimized configuration	O-fcc	O-hcp	O-top	O-fcc	O-fcc	O-top	O-fcc	O-bridge	O-top	O-fcc	O-hcp	O-bridge
adsorption energy	−2.19	−2.05	−1.82	−1.99	−2.10	−1.73	−1.57	−1.94	−1.34	−3.25	−3.09	−3.20

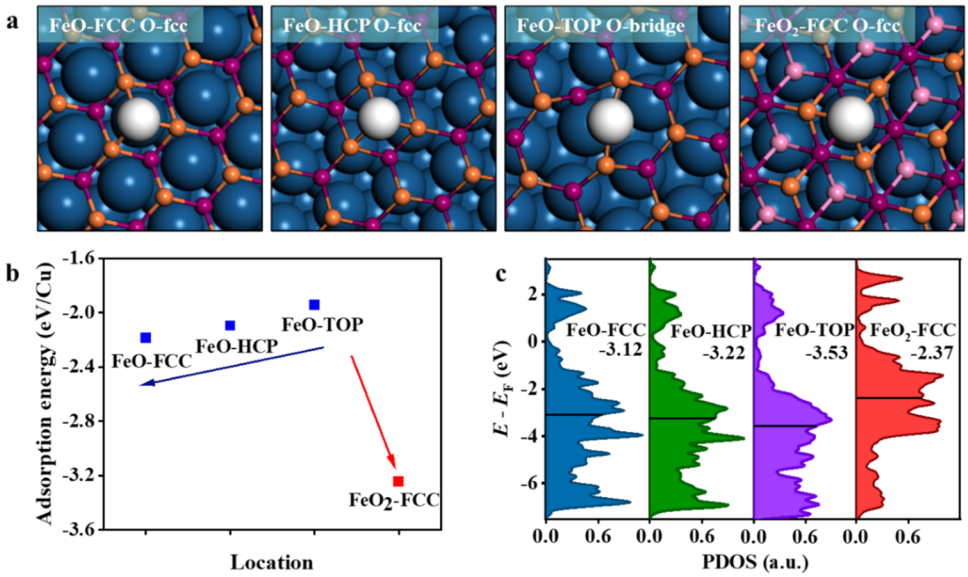

Figure 4. (a) Optimized configurations of the most stable Cu adsorption sites in the three domains of FeO/Pt(111) and the FCC domain of FeO_{2-x}/Pt(111). Pt: dark blue; Fe: purple; surface O: orange; interface O: pink; and Cu: white. (b) Adsorption energies of Cu location on the three domains of FeO/Pt(111) and the FCC domain of FeO_{2-x}/Pt(111). (c) Projected density of states (PDOS) for *p*-orbitals of surface O in the three domains of FeO/Pt(111) and the FCC domain of FeO_{2-x}/Pt(111). Inserted values denote the positions of the *p*-band center (ε_p).

originate from the aggregated Cu atoms, which preferentially nucleate at the FeO domain boundaries and further diffuse through the FeO film.

Depositing Cu on the FeO_{2-x}/Pt(111) surface at RT can still produce ordered nanostructures (Figure 3b). Most clusters contain more than one atom (Figure 3c) and have two different apparent heights of 0.16 and 0.20 nm (Figure 3d). Compared with the Cu nanostructures deposited on FeO_{2-x} at 100 K, the lower cluster density (0.15 count/nm^2) and larger aggregates of Cu atoms have been observed on the surface with Cu deposited at RT. However, the dispersion of Cu on FeO_{2-x} is much higher than that on FeO in the case of RT deposition, suggesting a stronger interaction between Cu and FeO_{2-x} than FeO. Figure 3c shows that most Cu clusters are still located at FeO_2-FCC domains and a few Cu clusters are observed on HCP domains, similar to the phenomenon of deposited Cu on FeO_{2-x} at 100 K.

XPS measurements were performed to figure out the valence states of Cu overlayers grown on FeO and FeO_{2-x}. To increase the XPS signal intensity, the deposited Cu coverage is increased to 0.5 ML (Figure 3e). No shakeup satellites around 942.0 eV characteristic for Cu^{2+} are observed in all Cu 2p spectra, which excludes the presence of Cu^{2+} species.[53] Further, Cu 2p BE of the Cu/FeO_{2-x} surface is 0.3 eV lower than that of the Cu/FeO surface. Since the Cu 2p BE difference between Cu^0 and Cu^+ is about 0.1 eV, the 0.3 eV BE difference might derive from different interfacial charge transfers and size effects.[54] Cu LVV Auger peaks are used to distinguish the valence states, confirming the coexistence of Cu^0 (918.0 eV) and Cu^+ (915.8 eV) species on the Cu/FeO and Cu/FeO_{2-x} surfaces (Figure 3f).[53] Deposited Cu atoms on FeO and FeO_{2-x} films are both partially oxidized, which derives from the charge transfer at the Cu−FeO_x interfaces. The proportion of Cu^+ on Cu/FeO_{2-x} is much higher, which indicates that more electrons of Cu are transferred to FeO_{2-x}, and the Cu−FeO_{2-x} interaction is stronger than Cu−FeO.

Theoretical Analysis of Cu on FeO/Pt(111) and FeO_{2-x}/Pt(111)

DFT calculations were carried out to figure out the geometric structures of single-atom Cu located on FeO/Pt(111) and FeO_{2-x}/Pt(111) surfaces and to unravel the nature of metal-oxide interactions. We first investigate the stability of Cu atoms at O-fcc, O-hcp, and O-top sites in the three domains of FeO/Pt(111) and FCC domains of FeO_{2-x}/Pt(111) (Figure S6). The optimized configurations and the adsorption energies (E_{ads}, see the Methods Section) for Cu adsorbed on a total of 12 sites are summarized in Table 1. In the FeO-FCC domain, the most stable Cu location is found at the O-fcc site (Figure 4a) with an adsorption energy of −2.19 eV. In the FeO-HCP domain, only O-fcc and O-top sites are obtained because the Cu atom initially placed at the O-hcp site is spontaneously relaxed to the most favorable O-fcc site (E_{ads} = −2.10 eV). In the FeO-TOP domain, it is found that Cu located at the O-hcp site can evolve into an O-bridge site where the Cu adatom is coordinated by two oxygen atoms, whose stability (E_{ads} = −1.94 eV) exceeds those at O-fcc and O-top sites. In the FeO_2-FCC domain, Cu located at the O-fcc site is favored with the adsorption energy of −3.25 eV compared with O-hcp and O-bridge sites. Note that the Cu atom initially put at the O-top site is relaxed to the O-bridge site. Therefore, the thermodynamic stability of Cu adsorption sites on the FeO/Pt(111) and FeO_{2-x}/Pt(111) surfaces follows an order of

https://doi.org/10.1021/jacsau.2c00580
JACS Au 2023, 3, 176−184

FeO_2-FCC > FeO-FCC > FeO-HCP > FeO-TOP, as shown in Figure 4b. This calculated trend well explains the STM observation that Cu preferentially sits on FCC domains of both FeO/Pt(111) and FeO_{2-x}/Pt(111) surfaces, and Cu interacts more strongly with the FeO_{2-x}/Pt(111) surface than with the FeO/Pt(111) surface.

The reactivity of surface O is mainly dependent on its electronic structure, which can be reflected by the density of states (DOS) population and quantitatively described by the *p*-band center.[55−57] Figure 4c shows the *p*-orbitals projected density of states (PDOS) of surface O atoms in different regions of the FeO_x/Pt(111). Surface O in the FeO_2 domain exhibits a richer DOS population around the Fermi level compared to that of FeO, which qualitatively indicates a high reactivity of surface O in the FeO_2 domain. Through quantifying the *p*-band center (ε_p) of surface O (see Methods Section for the formula), we find that surface O in FeO_2-FCC possesses a higher ε_p (−2.37 eV) than that in FeO/Pt(111) indicating the highest interaction with Cu adsorption. Furthermore, ε_p values of surface O are −3.12 eV for FeO-FCC, −3.22 eV for FeO-HCP, and −3.53 eV for FeO-TOP, respectively. It is well consistent with the interaction order of surface O in different regions of FeO_x/Pt(111) with the Cu adatom, i.e., FeO_2-FCC > FeO-FCC > FeO-HCP > FeO-TOP. The increase of surface O reactivity in the FCC domain of the FeO film stems from the enhancement of the interfacial Fe−Pt bond strength, i.e., the shorter spatial separation between the FeO overlayer and Pt substrate and the stronger charge transfer.[48] As for the FeO_2 domain, the Fe−Pt bonding at the FeO/Pt interface is replaced by much stronger Fe−O binding, inducing a higher reactivity of the surface O. Therefore, we conclude that the electronic effect plays a dominant role in Cu interaction with surface O where the surface O atom with the more positive *p*-band center can enhance adsorption of Cu.

Discussion

Depositing Cu on the FeO/Pt(111) surface at 100 K and RT produces highly dispersed cluster arrays and aggregated linear nanostructures, respectively. At 100 K, Cu atoms have limited diffusion ability to avoid further agglomeration and reside at the lowest energy domains (FCC domains). However, at RT, Cu atoms can nucleate and aggregate at the defect sites such as domain boundaries, which indicates a weak interaction between Cu atoms and the FeO surface. As a result, the regular distribution of Cu atoms and clusters on the FeO film at 100 K is from both preferential bonding at FCC domains and limited diffusion ability at this temperature. Deposition of Cu on the FeO_{2-x}/Pt(111) surface at both 100 K and RT produces Cu clusters with a regular spatial distribution. Most Cu atoms are observed to selectively locate on FeO_2-FCC domains. A higher dispersion degree of Cu atoms on the FeO_{2-x} film indicates the limited migration of Cu atoms over FeO_2 domains and the stronger interaction between Cu atoms and FeO_2, which has been validated by XPS and DFT results.

The FeO/Pt(111) and FeO_{2-x}/Pt(111) surfaces have the similar coordination structure of surface O atoms but show significantly different interactions with Cu adatoms. They both can be used as model catalysts to understand the influence of the reactivity of surface O atoms on the metal-oxide interaction. DFT calculation results show that Cu atoms on the FeO and FeO_2 surfaces all prefer to locate at the O-hollow site and thus have the same coordination environment. Therefore, the interaction between Cu atoms and FeO_x mainly depends on the property of surface O atoms, and the *p*-band center has been used as a descriptor to directly reflect their electronic properties. As reported in previous studies, the *p*-band center of surface O could be used as a descriptor for the reactivity of surface O for C−H activation.[56,57] Here, we find that surface O whose *p*-band center is closer to Fermi energy shows a higher bonding tendency with metals. As shown in Figure S7, a good and quantitative scaling relation exists between the ε_p and Cu−FeO_x interaction. The *p*-band center of surface O can be used as a new descriptor for metal-oxide interactions, which is helpful for the rational design of single-atom and cluster catalysts supported on oxides.

FeO/Pt(111) films can be used as templates for the construction of well-defined Cu cluster arrays only at 100 K, while deposition of Cu atoms on FeO_{2-x}/Pt(111) at 100 K and RT can form regular metal arrays. In addition, we find that Ce atoms are randomly distributed on the FeO film but form ordered cluster arrays on the FeO_{2-x} films at 100 K and RT (Figure S8). Due to the low reactivity of surface O of FeO, most of the metals have weak interactions with the FeO film and present low thermal stability, which results in the formation of aggregated nanostructures. Furthermore, the difference in the interaction between metals and different domains of the FeO film is small. Therefore, only Cu and Au cluster arrays with regular distribution form on the FeO film at low temperatures. In contrast, the FeO_2 domain with high surface O reactivity can have strong interactions with more metal atoms such as Ce resulting in highly dispersed metal clusters with relatively high thermal stability. In addition, the surface reactivity of the FeO_2 domain and surrounding FeO domain has a sufficiently large difference such that many metals have the tendency to locate at the FeO_2 domains forming periodic arrays. Therefore, the FeO_{2-x} film might be a more universal template for the construction of well-ordered metal cluster arrays in contrast with the FeO film.

CONCLUSIONS

FeO/Pt(111) and FeO_{2-x}/Pt(111) surfaces with moiré patterns are used as templates for the construction of well-ordered Cu cluster arrays at 100 K. Cu atoms deposited on FeO at RT aggregate significantly forming linear nanostructures, while the regular distribution of clusters can be observed after depositing Cu on FeO_{2-x} at RT. DFT calculation results show that Cu atoms prefer to locate at O-fcc sites of FCC domains of FeO and FeO_{2-x}. The adsorption strength of a single Cu atom on FeO/Pt(111) and FeO_{2-x}/Pt(111) follows an order of FeO_2-FCC > FeO-FCC > FeO-HCP > FeO-TOP, which can be correlated with the *p*-band center of the surface O. Therefore, the stronger interaction between Cu atoms and FeO_2 results from the higher surface O reactivity as described by the *p*-band center.

ASSOCIATED CONTENT

Supporting Information

The Supporting Information is available free of charge at https://pubs.acs.org/doi/10.1021/jacsau.2c00580.

Extended results, including STM images, XPS data, and DFT models (PDF)

https://doi.org/10.1021/jacsau.2c00580
JACS Au 2023, 3, 176−184

AUTHOR INFORMATION

Corresponding Authors

Yanxiao Ning − *State Key Laboratory of Catalysis, iChEM, Dalian Institute of Chemical Physics, Chinese Academy of Sciences, Dalian 116023, China*; Email: yxning@dicp.ac.cn

Qiang Fu − *State Key Laboratory of Catalysis, iChEM, Dalian Institute of Chemical Physics, Chinese Academy of Sciences, Dalian 116023, China; Dalian National Laboratory for Clean Energy, Dalian Institute of Chemical Physics, Chinese Academy of Sciences, Dalian 116023, China;* orcid.org/0000-0001-5316-6758; Email: qfu@dicp.ac.cn

Authors

Xuda Luo − *State Key Laboratory of Catalysis, iChEM, Dalian Institute of Chemical Physics, Chinese Academy of Sciences, Dalian 116023, China; University of Chinese Academy of Sciences, Beijing 100049, China*

Xiaoyuan Sun − *State Key Laboratory of Catalysis, iChEM, Dalian Institute of Chemical Physics, Chinese Academy of Sciences, Dalian 116023, China; Zhang Dayu School of Chemistry, Dalian University of Technology, Dalian 116024, China*

Zhiyu Yi − *State Key Laboratory of Catalysis, iChEM, Dalian Institute of Chemical Physics, Chinese Academy of Sciences, Dalian 116023, China; University of Chinese Academy of Sciences, Beijing 100049, China*

Le Lin − *State Key Laboratory of Catalysis, iChEM, Dalian Institute of Chemical Physics, Chinese Academy of Sciences, Dalian 116023, China*

Xinhe Bao − *State Key Laboratory of Catalysis, iChEM, Dalian Institute of Chemical Physics, Chinese Academy of Sciences, Dalian 116023, China; Dalian National Laboratory for Clean Energy, Dalian Institute of Chemical Physics, Chinese Academy of Sciences, Dalian 116023, China;* orcid.org/0000-0001-9404-6429

Complete contact information is available at: https://pubs.acs.org/10.1021/jacsau.2c00580

Author Contributions

X.L., Y.N., and Q.F. conceived and designed the experiments; X.L. and Z.Y. carried out the preparation of experimental samples and STM and XPS characterizations; X.S. and L.L. carried out DFT calculations; and X.L. and X.S. drafted the original manuscript; All authors, including X.L., X.S., Z.Y., L.L., Y.N., Q.F., and X.B., contributed to the analysis, interpretation, discussion of results, and the revisions of the manuscript. CRediT: **Xuda Luo** data curation, formal analysis, investigation, methodology, writing-original draft, writing-review & editing; **Xiaoyuan Sun** data curation, formal analysis, investigation, writing-original draft; **Zhiyu Yi** data curation, formal analysis, investigation, writing-review & editing; **Le Lin** formal analysis, methodology, writing-original draft, writing-review & editing; **Yanxiao Ning** conceptualization, formal analysis, investigation, supervision, writing-original draft, writing-review & editing; **Qiang Fu** conceptualization, funding acquisition, methodology, project administration, supervision, writing-review & editing; **Xinhe Bao** conceptualization, funding acquisition, project administration, writing-review & editing.

Notes

The authors declare no competing financial interest.

ACKNOWLEDGMENTS

This work was financially supported by the National Key R&D Program of China (2021YFA1502800), National Natural Science Foundation of China (Nos. 21825203, 22288201, and 91945302), Photon Science Center for Carbon Neutrality, and Liaoning Revitalization Talents Program (XLYC1902117).

REFERENCES

(1) Liu, L.; Corma, A. Metal Catalysts for Heterogeneous Catalysis: From Single Atoms to Nanoclusters and Nanoparticles. *Chem. Rev.* **2018**, *118*, 4981−5079.

(2) Dong, C.; Li, Y.; Cheng, D.; Zhang, M.; Liu, J.; Wang, Y.-G.; Xiao, D.; Ma, D. Supported Metal Clusters: Fabrication and Application in Heterogeneous Catalysis. *ACS Catal.* **2020**, *10*, 11011−11045.

(3) Lang, R.; Du, X.; Huang, Y.; Jiang, X.; Zhang, Q.; Guo, Y.; Liu, K.; Qiao, B.; Wang, A.; Zhang, T. Single-Atom Catalysts Based on the Metal-Oxide Interaction. *Chem. Rev.* **2020**, *120*, 11986−12043.

(4) Li, J.; Guan, Q.; Wu, H.; Liu, W.; Lin, Y.; Sun, Z.; Ye, X.; Zheng, X.; Pan, H.; Zhu, J.; Chen, S.; Zhang, W.; Wei, S.; Lu, J. Highly Active and Stable Metal Single-Atom Catalysts Achieved by Strong Electronic Metal-Support Interactions. *J. Am. Chem. Soc.* **2019**, *141*, 14515−14519.

(5) van Deelen, T. W.; Mejía, C. H.; de Jong, K. P. Control of metal-support interactions in heterogeneous catalysts to enhance activity and selectivity. *Nat. Catal.* **2019**, *2*, 955−970.

(6) Zhang, J.; Wang, Z.; Chen, W.; Xiong, Y.; Cheong, W.-C.; Zheng, L.; Yan, W.; Gu, L.; Chen, C.; Peng, Q.; Hu, P.; Wang, D.; Li, Y. Tuning Polarity of Cu-O Bond in Heterogeneous Cu Catalyst to Promote Additive-free Hydroboration of Alkynes. *Chem* **2020**, *6*, 725−737.

(7) Fu, Q.; Li, W.-X.; Yao, Y.; Liu, H.; Su, H.-Y.; Ma, D.; Gu, X.-K.; Chen, L.; Wang, Z.; Zhang, H.; Wang, B.; Bao, X. Interface-Confined Ferrous Centers for Catalytic Oxidation. *Science* **2010**, *328*, 1141−1144.

(8) Kim, T.-S.; Kim, J.; Song, H. C.; Kim, D.; Jeong, B.; Lee, J.; Shin, J. W.; Ryoo, R.; Park, J. Y. Catalytic Synergy on PtNi Bimetal Catalysts Driven by Interfacial Intermediate Structures. *ACS Catal.* **2020**, *10*, 10459−10467.

(9) Wu, C. H.; Liu, C.; Su, D.; Xin, H. L.; Fang, H.-T.; Eren, B.; Zhang, S.; Murray, C. B.; Salmeron, M. B. Bimetallic synergy in cobalt−palladium nanocatalysts for CO oxidation. *Nat. Catal.* **2019**, *2*, 78−85.

(10) Xu, Z.; Zhang, Y.; Qin, L.; Meng, Q.; Xue, Z.; Qiu, L.; Zhang, G.; Guo, X.; Li, Q. Crystal Facet Induced Single-Atom Pd/Co_xO_y on a Tunable Metal-Support Interface for Low Temperature Catalytic Oxidation. *Small* **2020**, *16*, No. e2002071.

(11) Song, B.; Choi, D.; Xin, Y.; Bowers, C. R.; Hagelin-Weaver, H. Ultra-Low Loading Pt/CeO_2 Catalysts: Ceria Facet Effect Affords Improved Pairwise Selectivity for Parahydrogen Enhanced NMR Spectroscopy. *Angew. Chem., Int. Ed.* **2021**, *60*, 4038−4042.

(12) Wan, J.; Chen, W.; Jia, C.; Zheng, L.; Dong, J.; Zheng, X.; Wang, Y.; Yan, W.; Chen, C.; Peng, Q.; Wang, D.; Li, Y. Defect Effects on TiO_2 Nanosheets: Stabilizing Single Atomic Site Au and Promoting Catalytic Properties. *Adv. Mater.* **2018**, *30*, No. 1705369.

(13) Liu, N.; Ma, X.-L.; Li, J.; Xiao, H. Singly Dispersed Bimetallic Sites as Stable and Efficient Single-Cluster Catalysts for Activating N_2 and CO_2. *J. Phys. Chem. C* **2021**, *125*, 27192−27198.

(14) Liu, P.; Zhao, Y.; Qin, R.; Mo, S.; Chen, G.; Gu, L.; Chevrier, D. M.; Zhang, P.; Guo, Q.; Zang, D.; Wu, B.; Fu, G.; Zheng, N. Photochemical route for synthesizing atomically dispersed palladium catalysts. *Science* **2016**, *352*, 797−800.

(15) Matthey, D.; Wang, J. G.; Wendt, S.; Matthiesen, J.; Schaub, R.; Lægsgaard, E.; Hammer, B.; Besenbacher, F. Enhanced Bonding of Gold Nanoparticles on Oxidized TiO_2(110). *Science* **2007**, *315*, 1692−1696.

(16) Yim, C. M.; Lamoureux, P. S.; Mellor, A.; Pang, C. L.; Idriss, H.; Pacchioni, G.; Thornton, G. Size and Shape Dependence of the

Electronic Structure of Gold Nanoclusters on TiO_2. *J. Phys. Chem. Lett.* **2021**, *12*, 8363−8369.
(17) Hulva, J.; Meier, M.; Bliem, R.; Jakub, Z.; Kraushofer, F.; Schmid, M.; Diebold, U.; Franchini, C.; Parkinson Gareth, S. Unraveling CO adsorption on model single-atom catalysts. *Science* **2021**, *371*, 375−379.
(18) Liu, Y.; Han, Z.; Gewinner, S.; Schöllkopf, W.; Levchenko, S. V.; Kuhlenbeck, H.; Cuenya, B. R. Adatom Bonding Sites in a Nickel-Fe_3O_4(001) Single-Atom Model Catalyst and O_2 Reactivity Unveiled by Surface Action Spectroscopy with Infrared Free-Electron Laser Light. *Angew. Chem., Int. Ed.* **2022**, *61*, No. e202202561.
(19) Bruix, A.; Rodriguez, J. A.; Ramirez, P. J.; Senanayake, S. D.; Evans, J.; Park, J. B.; Stacchiola, D.; Liu, P.; Hrbek, J.; Illas, F. A new type of strong metal-support interaction and the production of H_2 through the transformation of water on Pt/CeO_2(111) and Pt/CeO_x/TiO_2(110) catalysts. *J. Am. Chem. Soc.* **2012**, *134*, 8968−8974.
(20) Therrien, A. J.; Hensley, A. J. R.; Marcinkowski, M. D.; Zhang, R.; Lucci, F. R.; Coughlin, B.; Schilling, A. C.; McEwen, J.-S.; Sykes, E. C. H. An atomic-scale view of single-site Pt catalysis for low-temperature CO oxidation. *Nat. Catal.* **2018**, *1*, 192−198.
(21) Zhou, J.; Pan, J.; Jin, Y.; Peng, Z.; Xu, Z.; Chen, Q.; Ren, P.; Zhou, X.; Wu, K. Single-Cation Catalyst: Ni Cation in Monolayered CuO for CO Oxidation. *J. Am. Chem. Soc.* **2022**, *144*, 8430−8433.
(22) Sterrer, M.; Risse, T.; Pozzoni, U. M.; Giordano, L.; Heyde, M.; Rust, H. P.; Pacchioni, G.; Freund, H. J. Control of the charge state of metal atoms on thin MgO films. *Phys. Rev. Lett.* **2007**, *98*, No. 096107.
(23) Henry, C. R. 2D-Arrays of Nanoparticles as Model Catalysts. *Catal. Lett.* **2015**, *145*, 731−749.
(24) Zhang, H.; Fu, Q.; Cui, Y.; Tan, D.; Bao, X. Fabrication of metal nanoclusters on graphene grown on Ru(0001). *Chin. Sci. Bull.* **2009**, *54*, 2446−2450.
(25) Linas, S.; Jean, F.; Zhou, T.; Albin, C.; Renaud, G.; Bardotti, L.; Tournus, F. Moire induced organization of size-selected Pt clusters soft landed on epitaxial graphene. *Sci. Rep.* **2015**, *5*, No. 13053.
(26) Will, M.; Atodiresei, N.; Caciuc, V.; Valerius, P.; Herbig, C.; Michely, T. A Monolayer of Hexagonal Boron Nitride on Ir(111) as a Template for Cluster Superlattices. *ACS Nano* **2018**, *12*, 6871−6880.
(27) Auwärter, W. Hexagonal boron nitride monolayers on metal supports: Versatile templates for atoms, molecules and nanostructures. *Surf. Sci. Rep.* **2019**, *74*, 1−95.
(28) Rienks, E. D. L.; Nilius, N.; Rust, H.-P.; Freund, H.-J. Surface potential of a polar oxide film: FeO on Pt(111). *Phys. Rev. B* **2005**, *71*, No. 241404.
(29) Zhang, W.; Li, Z.; Luo, Y.; Yang, J. First Principles Study on the Geometric and Electronic Structures of the FeO/Pt(111) Surface. *J. Phys. Chem. C* **2009**, *113*, 8302−8305.
(30) Yao, Y.; Fu, Q.; Wang, Z.; Tan, D.; Bao, X. Growth and Characterization of Two-Dimensional FeO Nanoislands Supported on Pt(111). *J. Phys. Chem. C* **2010**, *114*, 17069−17079.
(31) Merte, L. R.; Grabow, L. C.; Peng, G.; Knudsen, J.; Zeuthen, H.; Kudernatsch, W.; Porsgaard, S.; Lægsgaard, E.; Mavrikakis, M.; Besenbacher, F. Tip-Dependent Scanning Tunneling Microscopy Imaging of Ultrathin FeO Films on Pt(111). *J. Phys. Chem. C* **2011**, *115*, 2089−2099.
(32) Liu, Y.; Ning, Y.; Yu, L.; Zhou, Z.; Liu, Q.; Zhang, Y.; Chen, H.; Xiao, J.; Liu, P.; Yang, F.; Bao, X. Structure and Electronic Properties of Interface-Confined Oxide Nanostructures. *ACS Nano* **2017**, *11*, 11449−11458.
(33) Nilius, N.; Rienks, E. D.; Rust, H. P.; Freund, H. J. Self-organization of gold atoms on a polar FeO(111) surface. *Phys. Rev. Lett.* **2005**, *95*, No. 066101.
(34) Giordano, L.; Pacchioni, G.; Goniakowski, J.; Nilius, N.; Rienks, E. D.; Freund, H. J. Charging of metal adatoms on ultrathin oxide films: Au and Pd on FeO/Pt(111). *Phys. Rev. Lett.* **2008**, *101*, No. 026102.
(35) Johansson, N.; Merte, L. R.; Grånäs, E.; Wendt, S.; Andersen, J. N.; Schnadt, J.; Knudsen, J. Oxidation of Ultrathin FeO(111) Grown on Pt(111): Spectroscopic Evidence for Hydroxylation. *Top. Catal.* **2016**, *59*, 506−515.
(36) Lewandowski, M.; Groot, I. M. N.; Shaikhutdinov, S.; Freund, H. J. Scanning tunneling microscopy evidence for the Mars-van Krevelen type mechanism of low temperature CO oxidation on an FeO(111) film on Pt(111). *Catal. Today* **2012**, *181*, 52−55.
(37) Merte, L. R.; Bai, Y.; Zeuthen, H.; Peng, G.; Lammich, L.; Besenbacher, F.; Mavrikakis, M.; Wendt, S. Identification of O-rich structures on platinum(111)-supported ultrathin iron oxide films. *Surf. Sci.* **2016**, *652*, 261−268.
(38) Sun, Y. N.; Giordano, L.; Goniakowski, J.; Lewandowski, M.; Qin, Z. H.; Noguera, C.; Shaikhutdinov, S.; Pacchioni, G.; Freund, H. J. The interplay between structure and CO oxidation catalysis on metal-supported ultrathin oxide films. *Angew. Chem., Int. Ed.* **2010**, *49*, 4418−4421.
(39) Wu, H.; Fu, Q.; Li, Y.; Cui, Y.; Wang, R.; Su, N.; Lin, L.; Dong, A.; Ning, Y.; Yang, F.; Bao, X. Controlled growth of uniform two-dimensional ZnO overlayers on Au(111) and surface hydroxylation. *Nano Res.* **2019**, *12*, 2348−2354.
(40) Yi, Z.; Lin, L.; Chang, Y.; Luo, X.; Gao, J.; Mu, R.; Ning, Y.; Fu, Q.; Bao, X. Dynamic transformation between bilayer islands and dinuclear clusters of Cr oxide on Au(111) through environment and interface effects. *Proc. Natl. Acad. Sci. U.S.A.* **2022**, *119*, No. e2120716119.
(41) Kresse, G.; Furthmüller, J. Efficiency of Ab-Initio Total Energy Calculations for Metals and Semiconductors using a Plane-Wave Basis Set. *Comp. Mater. Sci.* **1996**, *6*, 15−50.
(42) Perdew, J. P.; Burke, K.; Ernzerhof, M. Generalized Gradient Approximation Made Simple. *Phys. Rev. Lett.* **1996**, *77*, 3865−3868.
(43) Kresse, G.; Joubert, D. From Ultrasoft Pseudopotentials to the Projector Augmented-Wave Method. *Phys. Rev. B* **1999**, *59*, 1758−1775.
(44) Zeng, Z.; Chan, M. K. Y.; Zhao, Z.-J.; Kubal, J.; Fan, D.; Greeley, J. Towards First Principles-Based Prediction of Highly Accurate Electrochemical Pourbaix Diagrams. *J. Phys. Chem. C* **2015**, *119*, 18177−18187.
(45) Lin, L.; Zeng, Z.; Fu, Q.; Bao, X. Achieving flexible large-scale reactivity tuning by controlling the phase, thickness and support of two-dimensional ZnO. *Chem. Sci.* **2021**, *12*, 15284−15290.
(46) Zeng, Z.; Chang, K.-C.; Kubal, J.; Markovic, N. M.; Greeley, J. Stabilization of ultrathin (hydroxy)oxide films on transition metal substrates for electrochemical energy conversion. *Nat. Energy* **2017**, *2*, No. 17070.
(47) Ouyang, R.; Li, W.-X. First-principles study of the adsorption of Au atoms and Au_2 and Au_4 clusters on FeO/Pt(111). *Phys. Rev. B* **2011**, *84*, No. 165403.
(48) Sun, D.; Li, W. A first-principles study of the structure, electronic properties, and oxygen binding of FeO/Pt(111) and FeO_2/Pt(111). *Chin. J. Catal.* **2013**, *34*, 973−978.
(49) Kim, Y. J.; Westphal, C.; Ynzunza, R. X.; Wang, Z.; Galloway, H. C.; Salmeron, M.; Van Hove, M. A.; Fadley, C. S. The growth of iron oxide films on Pt(111): a combined XPD, STM, and LEED study. *Surf. Sci.* **1998**, *416*, 68−111.
(50) Ritter, M.; Ranke, W.; Weiss, W. Growth and structure of ultrathin FeO films on Pt(111) studied by STM and LEED. *Phys. Rev. B* **1998**, *57*, 7240−7251.
(51) Xu, L.; Zhang, W.; Zhang, Y.; Wu, Z.; Chen, B.; Jiang, Z.; Ma, Y.; Yang, J.; Huang, W. Oxygen Vacancy-Controlled Reactivity of Hydroxyls on an FeO(111) Monolayer Film. *J. Phys. Chem. C* **2011**, *115*, 6815−6824.
(52) Fu, Q.; Yao, Y.; Guo, X.; Wei, M.; Ning, Y.; Liu, H.; Yang, F.; Liu, Z.; Bao, X. Reversible structural transformation of FeO_x nanostructures on Pt under cycling redox conditions and its effect on oxidation catalysis. *Phys. Chem. Chem. Phys.* **2013**, *15*, 14708−14714.
(53) Tahir, D.; Tougaard, S. Electronic and optical properties of Cu, CuO and Cu_2O studied by electron spectroscopy. *J. Phys.: Condens. Matter* **2012**, *24*, No. 175002.
(54) Li, G.; Hu, S.; Xu, Q.; Zhu, J. Interaction between Cu Nanoparticles and CeO_2(111) Film Surfaces. *J. Phys. Chem. C* **2019**, *123*, 23563−23571.

https://doi.org/10.1021/jacsau.2c00580
JACS Au 2023, 3, 176−184

(55) Dickens, C. F.; Montoya, J. H.; Kulkarni, A. R.; Bajdich, M.; Nørskov, J. K. An electronic structure descriptor for oxygen reactivity at metal and metal-oxide surfaces. *Surf. Sci.* **2019**, *681*, 122−129.
(56) Jiang, C.; Song, H.; Sun, G.; Chang, X.; Zhen, S.; Wu, S.; Zhao, Z.-J.; Gong, J. Data-Driven Interpretable Descriptors for the Structure−Activity Relationship of Surface Lattice Oxygen on Doped Vanadium Oxides. *Angew. Chem., Int. Ed.* **2022**, *61*, No. e202206758.
(57) Xiong, C.; Chen, S.; Yang, P.; Zha, S.; Zhao, Z.-J.; Gong, J. Structure−Performance Relationships for Propane Dehydrogenation over Aluminum Supported Vanadium Oxide. *ACS Catal.* **2019**, *9*, 5816−5827.

https://doi.org/10.1021/jacsau.2c00580
JACS Au 2023, 3, 176−184